Clean Energy Science and Technology 2026, 4(2), 782.
doi: https://doi.org/10.18686/cest782

Article

Experimental tests of an oxy-fuel natural gas burner with CO_2 dilution at atmospheric pressure as model conditions for full-scale supercritical combustion

Sergey Osipov, Pavel Bryzgunov, Vadim Yakovlev*, Ilya Feoktistov, Nikolay Rogalev

Department of Innovative Technologies of High-Tech Industries (ITHTI), National Research University Moscow Power Engineering Institute (MPEI), Moscow 111250, Russia

*** Corresponding author:** Vadim Yakovlev, YakovlevVadS@mpei.ru

CITATION

Osipov S, Bryzgunov P, Yakovlev V, et al. Experimental tests of an oxy-fuel natural gas burner with CO_2 dilution at atmospheric pressure as model conditions for full-scale supercritical combustion. Clean Energy Science and Technology. 2026; 4(2): 782. https://doi.org/10.18686/cest782

ARTICLE INFO

Received: 27 February 2026
Revised: 26 March 2026
Accepted: 1 April 2026
Available online: 17 April 2026

Abstract: Direct-fired supercritical CO_2 cycles are one of the promising approaches to eliminate CO_2 emissions in the power energy sector, while maintaining high efficiency and the ability to burn fossil fuels. One of the key elements of such cycles is the combustor, in which natural gas is burned in an O_2/CO_2 environment at supercritical pressure. Oxy-fuel CO_2-diluted combustion differs significantly from traditional air-fuel combustion, which creates the need to adapt existing numerical modeling techniques. Experimental data are required to verify numerical methods, but present experimental studies are fragmented and non-formalized. This paper presents the results of an experimental test of the 15 kW oxy-fuel burner device in a tunnel gas furnace at atmospheric pressure. Experimental tests were carried out with oxygen-fuel ratios (α) of 1, 1.45, and 1.75 in the range of CO_2 mass fractions in the oxidizer (γ) from 0 to 0.9. An experimental temperature profile is obtained, the adiabatic combustion temperature is calculated, and the boundaries of stable combustion are determined. Based on the experimental results, the main similarity criteria of combustion were calculated, and it was shown that by changing the composition of the model mixture, it is possible to reduce the discrepancy of the similarity criteria between the model and full-scale oxy-fuel combustors.

Keywords: CO_2-diluted combustion; burner device; experimental test; normal conditions; combustion similarity

1. Introduction

According to 2024 data, the energy sector accounts for 29% of the global greenhouse gas emissions in CO_2-equivalent, making power plants the largest source of carbon pollution on Earth [1]. The increasing concentration of greenhouse gases in the planet's atmosphere leads to global warming, which is a source of concern for scientists and the public around the world. It is obviously impossible to resolve the global environmental crisis without eliminating the carbon footprint in the energy sector. For this reason, an active search is currently underway for ways to reduce CO_2 emissions from power plants. The transition to direct-fired supercritical CO_2 cycles is considered one of the promising ways to eliminate the carbon footprint in the energy sector, while preserving the ability to burn fossil fuels. The most efficient direct-fired CO_2 cycle is the Allam cycle, whose net efficiency can reach up to 59% (lower calorific value) [2], which makes direct-fired cycles not only an environmentally friendly, but also an economically promising and competitive technology.

One of the key elements of the direct-fired supercritical CO_2 cycles is the combustion chamber, in which a gaseous fuel burns at supercritical pressures up to 300 atm (in the Allam cycle) in an O_2/CO_2 environment. This significantly distinguishes oxy-fuel CO_2-diluted combustion from traditional air-fuel combustion. Carbon dioxide has a much higher heat capacity and a lower diffusion coefficient compared to nitrogen. In addition, CO_2 is not as chemically inert as nitrogen, participating in oxidation both directly (for example, through the reaction CO + OH = CO_2 + H) and indirectly as a collision partner in third-body reactions (see, for example, the kinetic mechanism GRI 3.0 [3]). Combined, the chemical and physical effects of CO_2 make it a much stronger combustion inhibitor than N_2. According to Komarov et al. and Hu et al. [4, 5], all other things equal, in a CO_2-diluted mixture, the laminar burning velocity is 2–6 times lower than in an N_2-diluted mixture (see **Figure 1** for example). Thus, due to the use of CO_2 as the diluent, the existing methods of designing combustion chambers may not be applicable for direct-fired CO_2 cycles. Therefore, the experimental investigation of supercritical oxy-fuel CO_2-diluted combustion is needed to verify numerical modeling methods for designing combustion chambers of the direct-fired supercritical CO_2 cycles.

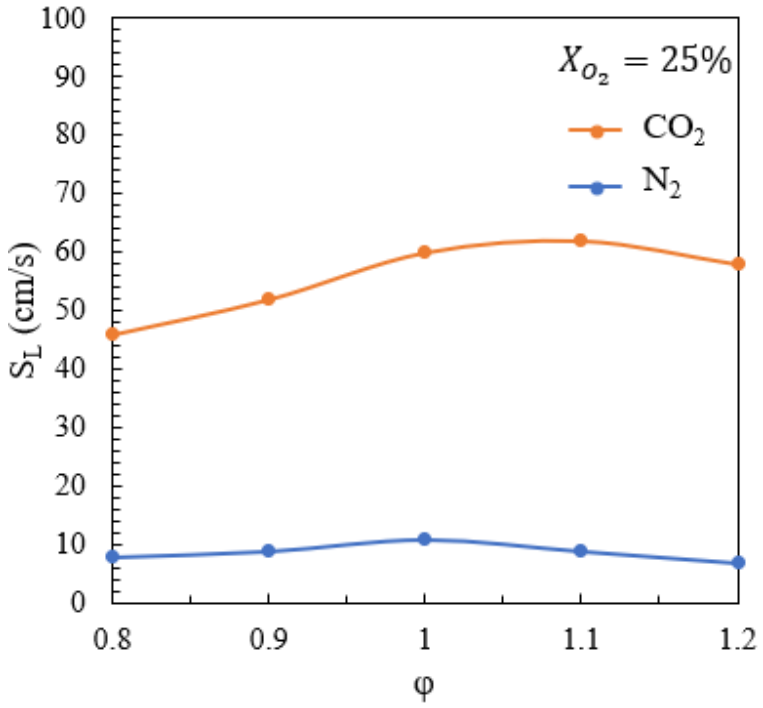

Figure 1. Dependence of laminar burning velocity on ϕ for CO_2- and N_2-diluted methane mixtures, $X_{O_2} = \frac{O_2}{O_2+CO_2(N_2)} = 25\%$.

Source: data taken from Hu et al. [5].

Currently, the experimental data on supercritical CO_2-diluted combustion, especially full-scale combustion chamber tests, are rather limited. The reason for this is the extremely high cost and danger of such experiments. In addition, all known experimental tests of oxy-fuel combustion chambers under supercritical conditions are conducted by private companies. For this reason, it is unlikely that detailed experimental data can be made available on request for validation of mathematical models. In 2015, Toshiba presented the first results on the development of a turbine

and combustion chamber for a demonstration plant operating on the Allam cycle [6]. The article provides a 3D model of the tested combustion chamber, but its internal structure is not shown or described. The test conditions and detailed test results are also not provided. We only know that the combustion chamber had successfully achieved the operating parameters (29.5 MPa, 1,350 °C at the outlet). In another 2015 article by Iwai et al. [7, 8], Toshiba presented more detailed test results of the Allam cycle combustion chamber under supercritical conditions (29 MPa, 1,400 °C). It has been established that stable supercritical oxy-fuel combustion is possible with an oxygen-fuel ratio up to 1.22 and CO_2 mass fractions in the oxidizer of up to 80%, but it is unknown whether these values are limiting. The article does not contain any experimental data that can be used as a basis for validating mathematical models. Both the English [7] and Japanese [8] versions of the article contain the results of CFD modeling of the combustion chamber, but the numerical data are presented only in the Japanese article. From it, we know that the maximum flame temperature is 2,350 °C, and the wall temperature is 750 °C. However, it is not possible to reproduce the results of CFD modeling, since the mathematical models used are not described (except for the RANS model of hydrodynamics) and not all the necessary initial data are known: the supply temperatures and flow rates of the components are not specified, and the geometric parameters of the combustion chamber and its burner are not given. Finally, in 2019 [9], Suzuki et al. presented the results of testing the oxy-fuel combustion chamber on a pilot Allam cycle power plant. The operating parameters of the combustion chamber were limited to a pressure of 10 MPa and an output temperature of 900 °C, which is much lower than the full-scale parameters of the Allam cycle (30 MPa, 1,100 °C). It is established that the temperature of the walls of the combustion chamber lies within the limits acceptable for the operation of the chamber material. However, the material itself is not named, and the exact values of the measured temperatures are not given ("low", "high"). Fuel underburning was also measured in dependence on the output temperature. At the maximum temperature (900 °C), emissions do not exceed 200 ppmvd for CO and 25 ppmvd for unburned hydrocarbons; the combustion completeness tends to 100%. However, the article lacks the initial data for numerical modeling: the temperatures of the components, their flow rates, the O_2–CO_2 ratio, and the equivalence coefficient. The internal structure of the combustor is also not clear. No other experimental tests of oxy-fuel combustion chambers in a supercritical CO_2-diluted environment have been found in the available literature.

As for model experiments conducted under conditions different from the full-scale ones, the possibility of extending their results to full-scale combustion has not been sufficiently investigated. In the existing tests of model combustion chambers, the possibility of scaling the results obtained to supercritical conditions is not considered. In 2014 [10], Anderson et al. presented the test results of an oxy-fuel superheater designed to operate at a pressure of 16 bar in their own direct-fired cycler cycle. Compared to the Allam cycle, the CES cycle operates at a lower pressure (up to 120 bar), has intermediate overheating between the high and medium pressure cylinders of the turbine, and is able to operate not only on carbon dioxide, but also on steam.

Unfortunately, the experimental data obtained are limited and cannot be used to validate mathematical models. It is also unlikely to be possible to obtain more detailed data from the authors themselves since CES is also a private company, and the technology is clearly for commercial use. Also, the possibility of scaling the obtained results to supercritical conditions was not considered in the article. In a 2017 article by Saanum and Ditaranto [11], the authors investigated oxy-fuel CO_2-diluted combustion in a vertical tubular combustion chamber. The combustion chamber was made of transparent quartz, which made it possible to visually observe the structure of the flame. Pressure (1–10 bar), thermal power (10–100 kW), oxygen excess, and O_2 volume fractions in the oxidizer (O_2/CO_2 mixture) were used as varied parameters. In dependence on these parameters, the diagrams of combustion modes were obtained, and CO emissions were measured. However, the possibility of extending the obtained results to supercritical conditions is not considered.

The possibility of transferring the results of model experiments to full-scale conditions (that is, from the laboratory to the industrial level) is discussed in the article by Weber and Mancini [12]. Based on the analysis of existing studies, the authors concluded that the main obstacle to transferring laboratory test results to the industrial level is the different nature of the processes. At the laboratory level, there is a strong interaction of turbulence and chemical kinetics. At the same time, on the industrial scale, turbulent mixing is the dominant process due to the inevitable increase in fuel and oxidizer flow rates. The authors conclude that, in general, for 2020 (the time of writing), this issue is not satisfactorily investigated. Thus, the results of model experiments cannot be directly extended to full-scale conditions. However, as shown in the article by Prieler et al. [13], the results of model experiments can be used to calibrate mathematical models for CFD-modelling in full-scale conditions. The Steady Flamelet Model showed good accuracy in modeling temperature (discrepancy is only 16 K) and heat flow (discrepancy is no more than 9.5%) for a small laboratory-scale furnace. When using this model on an industrial furnace with a capacity of 18.2 MW, the discrepancy between the simulated heat flow and the calculated one was only 1.9%. However, in order to verify the applicability of mathematical models verified on model conditions to full-scale conditions, it is necessary to ensure the similarity of combustion.

An attempt to study the similarity of combustion between model and full-scale combustors was made in 2024 [14]. For the full-scale conditions, the authors used the results of CFD modeling of the Allam cycle combustion chamber under supercritical pressure of 30 MPa and heat capacity of 105 MW; pressure and heat capacity were used as varied parameters. Eu, Sc, Re, Pr, M, and Le were considered as the main similarity criteria. Similarity in all the parameters under consideration was achieved with a model burner power of 800 kW (while the power of the full-scale chamber was reduced to 3.5 MW), pressure of 10 MPa, and initial fuel velocity of 50 m/s. Another study on combustion similarity was presented in 2025 [15]. A 15 kW burner device operating at a pressure of 30 MPa and an initial temperature of 895 K (Allam cycle) was used as full-scale conditions. For the model conditions, the same burner operating under normal conditions (0.1 MPa, 293 K) was used. The calculation was carried out theoretically. Based on the analysis of the differential equations of gas

dynamics and heat and mass transfer, Re, Eu, Pe (replaced by Pr, since Pe = Re · Pr), Bo, Sh (replaced by Sc, since Sh = f (Re, Sc)), Da_1, and Da_3 were adopted as the main similarity criteria for combustion processes. It has been found that when the power of the model burner is reduced to 12.5 kW, the similarity of hydrodynamics (Re, Eu) is achieved, and when it is reduced to 4 kW, the similarity of heat exchange (Pe, Bo, Da_3) is achieved, but the similarity of hydrodynamics is violated. The similarity of mass transfer is achieved at 12.5 kW for Sc and at 1.5 kW for Da_1. Thus, it is impossible to achieve the similarity of combustion simultaneously to all important criteria by changing the power of the model burner. However, it is possible to achieve similarity in individual processes (hydrodynamics, heat transfer), which makes it possible to validate mathematical models based on several separate tests under different conditions. In addition, the effect of such parameters as temperature, oxygen excess, and degree of dilution on the similarity of combustion has not been investigated. These parameters significantly affect the thermophysical properties of the fuel and the oxidizer, and therefore can also be used to achieve similarity of combustion.

Thus, existing studies of the operation of oxygen-fuel combustion chambers in supercritical conditions do not allow using their results to verify mathematical CFD models that can be used for their design. However, it is possible to verify mathematical models based on the results of tests conducted under conditions other than full-scale conditions, provided that the similarity of combustion processes between model and full-scale conditions is observed. Verified models can be used for CFD modelling of full-scale supercritical oxy-fuel combustion chambers. Although there are other numerical modelling methods besides CFD, such as density functional theory (DFT), molecular dynamics (MD), microkinetic modelling, and various combinations of kinetic models with CFD [16–19], CFD modelling remains extremely important for the design of thermal engineering equipment at the macro level. For this reason, this article focuses on experimental research that can be used to verify mathematical CFD models. This article presents the results of testing a model oxy-fuel burner device with a capacity of 15 kW on a rectangular tunnel furnace. The purpose of the study was to test the operability of the developed burner under model conditions, and to experimentally study the effect of the composition of the fuel mixture on the similarity of combustion processes to replicate, as closely as possible, the operating conditions of a full-scale oxy-fuel combustion chamber (30 MPa) under atmospheric conditions, since conducting a full-scale experiment is extremely difficult and expensive. The experiment confirmed the operability of the burner device in the range α 1–1.75 and γ 0–0.7. The dependence of the similarity criteria on α and γ under experimental conditions was established, and a comparison was made with the calculated full-scale values. It is shown that changing the composition of the fuel mixture can significantly reduce the discrepancy of the similarity criteria between model and field conditions. In the future, the results of the study are planned to be used to verify the methodology of numerical simulation of oxy-fuel combustion.

2. Materials and methods

2.1. Experimental stand

The schematic diagram of the experimental stand is shown in **Figure 2**.

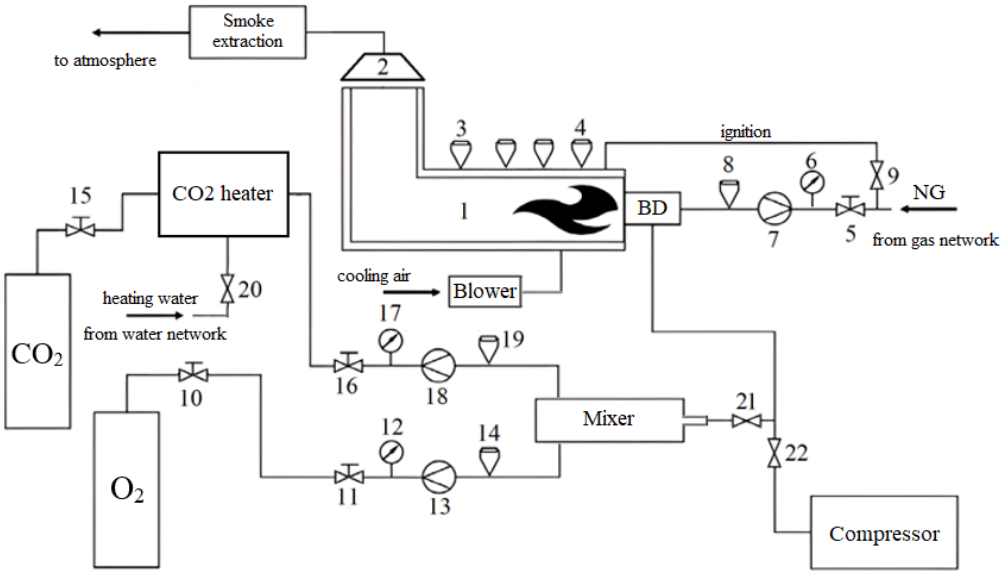

Figure 2. Schematic diagram of the experimental stand.

Note: 1—working section, 2—gas collecting hood, 3, 4—thermocouples for obtaining temperature profile in the working section, 5—natural gas valve, 6—natural gas pressure sensor, 7—natural gas flowmeter, 8—natural gas thermocouple, 9—natural gas valve for ignition, 10, 11—oxygen valves, 12—oxygen pressure sensor, 13—oxygen flowmeter, 14—oxygen thermocouple, 15, 16—CO_2 valves, 17—CO_2 pressure sensor, 18—CO_2 flowmeter, 19—CO_2 thermocouple, 20—heating water valve, 21—O_2/CO_2 mixture valve, 22—compressed air valve.

The working section 1 of the experimental stand, in which fuel is burned, is a rectangular tunnel furnace with a hydraulic diameter of 130 mm and an outlet section rotated 90°. This is done to facilitate the removal of flue gases and to provide an opportunity to observe the structure of the flame through the end window. On the side surface of the combustion chamber, two windows are also installed for visual observation of the flame structure. Fire-resistant glass is installed in all windows. The maximum capacity of the stand is limited to 15 kW due to restrictions on the consumption of natural gas coming from the network (1.5 m^3/h).

Thermal insulation of fireclay partition plates and fire-resistant bricks is provided to protect the tunnel furnace from thermal destruction. The outer casing of the combustion chamber is made of 3 mm thick stainless steel. The gap between the thermal insulation and the outer casing is 45 mm, and air is blown through to cool the combustion chamber. Flue gases and exhaust air are collected using a gas collecting hood 2 and then removed into the atmosphere using a smoke pump.

The temperature profile in the combustion chamber was measured during the test. To measure the temperature on the working section of the stand, four thermocouples 3 and 4, are provided. The layout of the points where the experimental temperature is measured is shown in **Figure 3**.

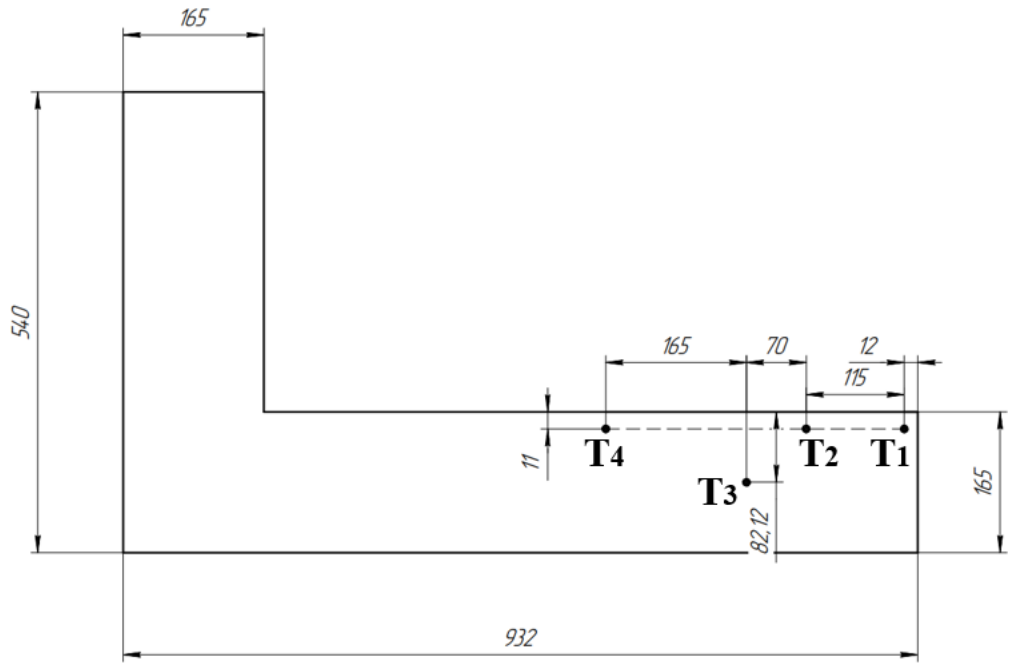

Figure 3. Diagram of the temperature measuring points in the working section of the experimental stand, all dimensions are in millimeters.

Initially, the stand also used a gas analyzer to measure CO emissions at the outlet of the working section. However, the measurement uncertainty of the gas analyzer available in the laboratory turned out to be too large, which makes the measurement results unsuitable for analysis. Therefore, here and further, the results of measuring CO emissions are not given.

The fuel used is natural gas (NG) supplied to the burner device (BD) from the gas network. The gas flow rate is regulated by the valve 5 and is measured by the flow meter 7; the pressure and temperature of the gas are measured, respectively, by the pressure sensor 6 and the thermocouple 8. Part of the natural gas can be supplied to the ignition device using the valve 9. Pure oxygen coming from a ramp with O_2 balloons is used as an oxidizer; the ramp holds 5 balloons. The oxygen flow rate is regulated by the valves 10 and 11, the thermocouple 14 measures the oxygen temperature, and the pressure and flow rate are measured by the pressure sensor 12 and the flow meter 13, respectively. In the mixer, oxygen is mixed with carbon dioxide, which comes from a ramp with CO_2 balloons; the ramp holds 10 balloons. The CO_2 flow rate is regulated by valves 15 and 16 and is measured by a flow meter 18. The pressure sensor 17 and the thermocouple 19 measure the pressure and temperature of CO_2. Standard 40 L gas balloons with a working pressure of 16 MPa were used to supply both O_2 and CO_2.

At a pressure of 16 MPa and room temperature, CO_2 is in a liquid state, while O_2 is in a supercritical state. To conduct the experiment in atmospheric conditions, it was necessary to reduce the pressure of O_2 and CO_2 to atmospheric pressure, which was carried out using throttling. However, when the pressure decreases to 1 atm, the transition of CO_2 from the liquid phase to the vapor phase occurs, which is accompanied by boiling and rapid cooling of carbon dioxide to a temperature below 0 °C. To eliminate the possibility of flame extinction due to the low temperature of carbon dioxide, a CO_2 heater is provided in the stand. The heater is a coil heat exchanger

immersed in a container with water heated by a thermoelectric heater (TEH) with a thermal power of 1.5 kW. The coil heat exchanger is made of a thin copper tube with an outer diameter of 6.2 mm and a wall thickness of 0.8 mm. The number of turns is 14, and each turn has a diameter of 135 mm. The estimated CO_2 inlet temperature is −27 °C, and CO_2 is supplied and discharged through 9 mm diameter fittings. The water container, the heater placed in, is a plastic tank with a volume of 20 L. The heating water enters the tank from the water network; its supply is regulated by a valve 20. The temperature of the heating water was not controlled—the heater's operation was adjusted according to the temperature of CO_2, measured by the thermocouple 19. The coil heat exchanger is presented in **Figure 4**.

Figure 4. A coil heat exchanger is used to heat carbon dioxide.

In the stand, a mixer is provided to mix oxygen and CO_2 to form a homogeneous oxidizing mixture. The mixer is a circular tube with a length of 1,000 mm and a diameter of 50 mm, where oxygen and CO_2 are supplied through two tangentially arranged tubes with a diameter of 9 mm. To improve mixing and make it possible to connect a standard gas hose to the mixer, a narrow tube with a diameter of 9 mm and a length of 100 mm is welded to the end of the mixer. The total length of the mixer is sufficient to ensure high-quality mixing of the oxidizer and diluent. The supply of the carbon dioxide-oxygen mixture is regulated by valve 21.

In addition to oxy-fuel combustion, the experimental stand can also conduct air-fuel combustion. An air compressor is installed to supply oxidizing air. The air supply is regulated by valve 22. The built experimental stand is shown in **Figure 5**, while **Figure 6** shows the drawing of the working section of the experimental stand.

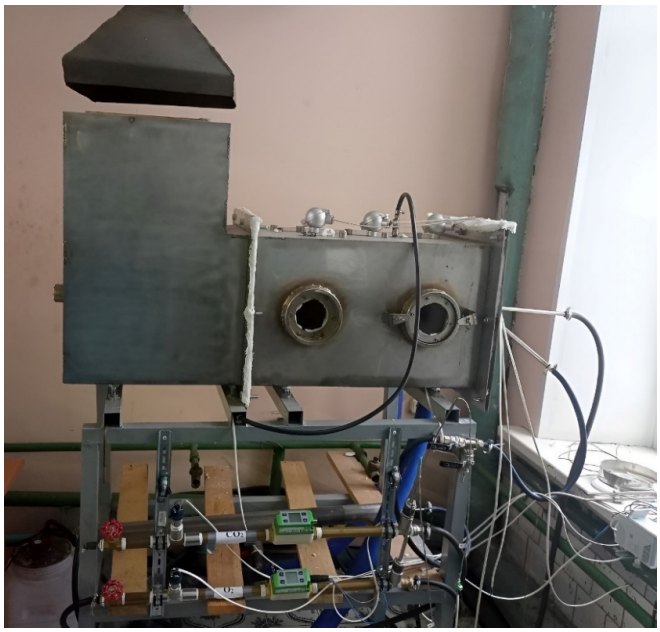

Figure 5. Built experimental stand.

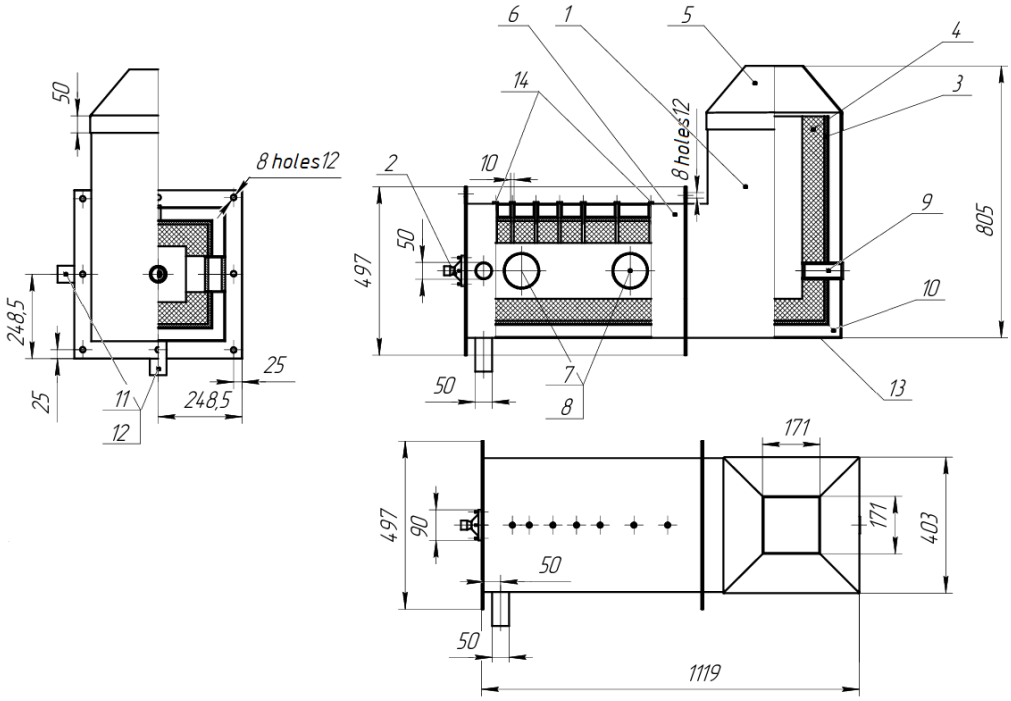

Figure 6. Drawing of the working section of the experimental stand, all dimensions are in millimeters.

Note: 1—vertical section, 2—burner device, 3—thermal insulation, 4—fireclay partition plates, 5—gas collecting hood, 6—horizontal section, 7, 8—sidewall observation windows, 9—endwall observation window, 10—gap between thermal insulation and outer casing, 11, 12—cooling air inlets, 13—outer casing, 14—fittings for installing thermocouples.

The object of the study was an oxy-fuel burner device developed by a team of authors from MPEI [20]. The burner device is a diffusion, pipe-in-pipe type, and consists of two parts: a fuel and oxidizer supply and mixing zone, and a diffuser zone. The fuel is supplied through the central channel, and the oxidizer (O_2/CO_2 mixture) is supplied through the outer annular channel. To improve the mixing of fuel and oxidizer, a blade swirl is installed in the annular channel, the central channel ends with a hemispherical perforated body, and the channels themselves are designed with a

smooth narrowing. After narrowing, the burner device smoothly expands in the diffuser area. Such a design of the burner makes it possible to stabilize the combustion and eliminate direct contact of the flame with the walls of the burner and the working section. The drawing and the prototype of the burner device are shown in **Figure 7**. **Table 1** summarizes the metrological characteristics of all measuring instruments.

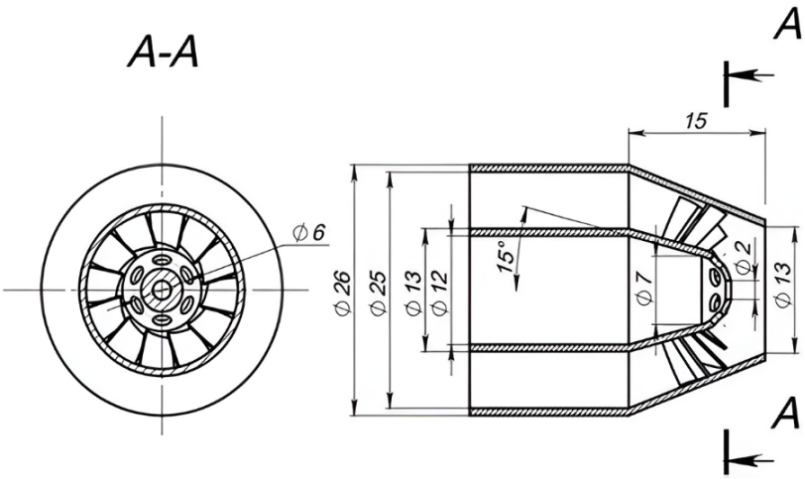

(a) Drawing of supply and mixing zone.

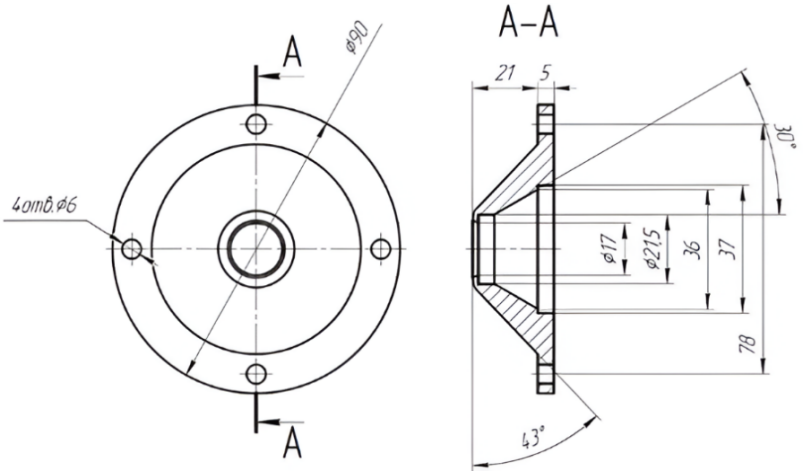

(b) Drawing of diffuser zone.

(c) Prototype.

Figure 7. Experimental burner device, all dimensions are in millimeters.

Table 1. Characteristics of measuring instruments.

Measured value	Instrument	Measurement limits	Source
Pressure of natural gas, oxygen, carbon dioxide	Measuring pressure transmitter PD100I-DA2.5-111-0.25 (ПД100И-ДА2,5-111-0,25)	Main reduced error: 0.25% (upper limit) Measuring range: 0.01–4.0 MPa Operating temperature range: −40–+100 °C	https://owen-kapo.ru//products/pd100i-da25-111-025 [21]
Temperature of natural gas, oxygen, carbon dioxide, flue gases	Thermoelectric transmitter DTPK254-17.80/200/0.5K.1 (ДТПК254-17.80/200/0,5К.1)	Measuring range: −40–+1,300 °C Main reduced error: 2.5 °C (−40–+333 °C). 0.75% (+333–+1,300 °C)	https://owen-kapo.ru//products/dtpk254-178020005k1 [22]
Flow rate of oxygen, carbon dioxide	EE741-A6D2AC2DN15	± (3% of measured value + 0.3% of upper limit) Measuring range: 0.2–76.3 norm. m^3/h	https://epluse.nt-rt.ru/images/manuals/EE741.pdf [23]
Temperature of flame	Thermoscope-300-2S-VT1 (Термоскоп-300-2С-ВТ1)	Temperature range. °C: 1,000–2,000 Main reduced error: ±0.75%	https://www.rospribor.com/files/698/195e21d202/tehnicheskie-harakteristiki-pirometra-termoskop-300-2c.pdf [24]
Temperature of flue gases in combustor	Thermoelectric transmitter DTPS021.1E-0.5/0.20 (ДТПS021.1Э-0,5/0,20)	Measuring range: from 0 °C to +1,600 °C Main reduced error: ±1.5 °C (0–600 °C). 0.25% (600–1,600 °C)	https://owen-prom.ru/products/dtps-termopary-iz-blagorodnykh-metallov/?mod=684275 [25]
Flow rate of natural gas	Flow sensor IZMERKON VA 520 1/2" (ИЗМЕРКОН VA 520 1/2")	Measuring range of velocity: up to 185.0 norm. m/s (0 °C; 1,013.25 mbar) Measuring range of flow rate: up to 50.0 norm. m^3/h (0 °C; 1,013.25 mbar) Main reduced error: ± (1.5% of measured value + 0.3% of upper limit)	https://air.by/upload/iblock/9a1/v3x126o3u9pi2den3ndn151f1qzxohbg.pdf?ysclid=mmxjojxsz2967028737 [26]

2.2. Test procedure

Due to the peculiarities of natural gas combustion in a CO_2 environment and the limited volumes of O_2 and CO_2, ignition and preheating of the tunnel furnace were carried out by air-fuel combustion. Since thermal insulation has a high heat absorption capacity, the preheating mode had to be maintained for up to 3 h before entering stationary operation, depending on the test. After the furnace went into stationary mode and the natural gas flow rate was set, switching from air to oxygen was carried out by gradually closing the air supply valve and opening the oxygen supply valve. To prevent flame separation due to the inhibitory effect of CO_2, pure oxygen is initially supplied to the main line. During further experiments, carbon dioxide is gradually supplied to the burner until the flame is extinguished.

Initially, the experimental test of the burner device was aimed at checking the operability in the range of (α) 1–1.75 and (γ) 0–0.9. A total of 3 series of tests were conducted, corresponding to (α) 1, 1.45, and 1.75. **Table 2** contains data on the experimental operating modes investigated in this work. In **Table 2**, there are no modes with γ greater than 0.7, since, as it turned out during the tests, the flame is extinguished at such values of γ.

During the tests, the readings of all measuring instruments were continuously recorded from the moment the stand was put into operation until it was turned off using a PLC. Based on the data obtained, continuous graphs of the values depending on time were drawn. The stationary mode of operation was fixed according to the formation of a "plateau" on the graph. The value of the measured value for a given mode was estimated by averaging on the corresponding plateau.

Table 2. Test modes of the burner device at atmospheric pressure.

Series of tests	Experimental conditions	Mode number in series					
		1	**2**	**3**	**4**	**5**	**6**
1	O_2 flow rate, m^3/h	2.89	2.73	2.65	2.85	2.87	2.89
	CO_2 flow rate, m^3/h	0	0.7	1.46	2.02	3.02	4.76
	Natural gas flow rate, m^3/h	1.42	1.48	1.49	1.49	1.47	1.53
	Natural gas temperature, °C	20					
	Oxidizer temperature, °C	44.5					
	γ	0	0.26	0.43	0.5	0.59	0.69
	α	1.01	0.92	0.88	0.95	0.97	0.94
2	O_2 flow rate, m^3/h	4.2	4.24	4.34	4.47	4.47	-
	CO_2 flow rate, m^3/h	0	0.52	1.12	2.58	4.32	-
	Natural gas flow rate, m^3/h	1.46	1.5	1.55	1.47	1.42	-
	Natural gas temperature, °C	20					
	Oxidizer temperature, °C	32.5					
	γ	0	0.14	0.26	0.44	0.57	-
	α	1.43	1.41	1.39	1.51	1.57	-
3	O_2 flow rate, m^3/h	5.12	5.6	5.89	5.52	5.48	5.68
	CO_2 flow rate, m^3/h	0	1.02	1.84	2.9	4.5	6
	Natural gas flow rate, m^3/h	1.6	1.57	1.67	1.63	1.51	1.48
	Natural gas temperature, °C	20					
	Oxidizer temperature, °C	44.5					
	γ	0	0.2	0.3	0.42	0.53	0.59
	α	1.59	1.78	1.76	1.69	1.81	1.91

In addition to the experimental temperature profiles, the maximum flame temperature for all operating modes was determined. For this purpose, the T3 thermocouple, which is closest to the flame, was used. The T3 thermocouple heats up from the radiation of the flame and at the same time emits thermal radiation onto the walls themselves. Since the maximum temperatures of the flame are usually very high (1,500–3,000 °C), and the flow rates of the components in the experimental stand are low due to low power (15 kW), convective heat exchange can be neglected. In this case, the maximum flame temperature can be calculated using the heat balance equation, which takes into account only radiative heat exchange:

$$\varepsilon_{\text{fl}} \cdot \left(T_{\text{fl}}^4 - T_3^4\right) = \varepsilon_{\text{therm}} \cdot \left(T_3^4 - T_{\text{w}}^4\right) \quad (1)$$

where T_{fl} is the maximum flame temperature, K;

T_3 is the temperature measured by the T3 thermocouple, K;

T_{w} is the temperature on the inner wall of thermal insulation, K;

$\varepsilon_{\text{therm}}$ is the T3 thermocouple emissivity factor;

ε_{fl} is the flame emissivity factor.

The left part of the heat balance equation corresponds to the heat transfer from the flame to the thermocouple, and the right part corresponds to the heat transfer from the thermocouple to the internal thermally insulated walls of the stand. The thermal insulation temperature on the inner walls was measured with a pyrometer; it was found that the temperature almost did not change during the tests and is about 670 K. The

emissivity factor of the thermocouple, taking into account the formation of soot, was assumed to be 1. The emissivity factor of the flame was determined from the reference data [27] according to the oxygen-fuel ratio (α). For test series No. 1 (α = 1) ε_{fl} = 0.09, for test series No. 2 and 3 (α = 1.45–1.75) ε_{fl} = 0.06.

3. Results and discussion

Figure 8 shows photographs of the flames taken through the endwall observation window, at various oxygen-fuel ratios (α) and CO_2 mass dilution in the oxidizer (γ). **Figure 9** shows photographs of flames taken through a sidewall observation window in a series of tests at α = 1. As can be seen from **Figures 5** and **6**, in the absence of CO_2 (γ = 0), that is, when burning in pure oxygen, the flame is the brightest and longest and has a white color, which indicates the maximum flame temperatures. As the CO_2 supply increases, the flame decreases in size and becomes more transparent. When γ is more than 0.4, at all values of α, the flame shifts close to the burner diffuser and acquires a translucent blue color, which indicates a strong decrease in underburning of the fuel. Although we were unable to obtain correct data on the amount of CO emissions, the conclusion that underburning decreases with an increase in α and/or γ is consistent with the research of third-party authors. For example, Saanum and Ditaranto [11] and Amato et al. [28] found that with an increase in the concentration of O_2 and CO_2 in the mixture, CO emissions indeed decrease. A similar result was obtained in the article by Li et al. [29] for kinetic modeling of methane combustion using the San Diego kinetic mechanism.

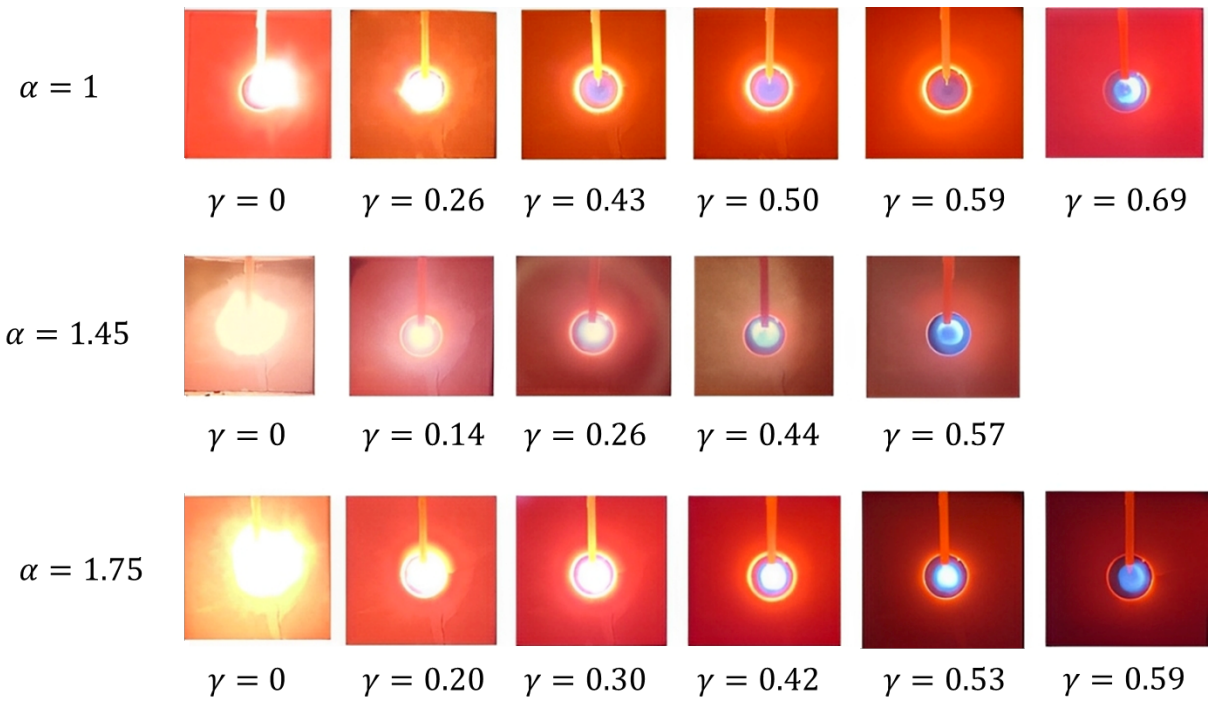

Figure 8. Flame photographs taken through the endwall observation window under various test conditions.

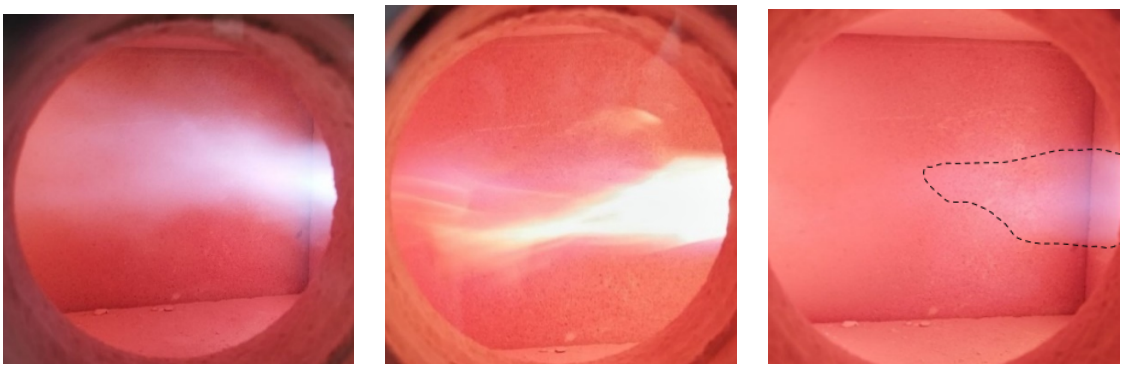

(a) γ = 0. **(b)** γ = 0.26. **(c)** γ = 0.43.

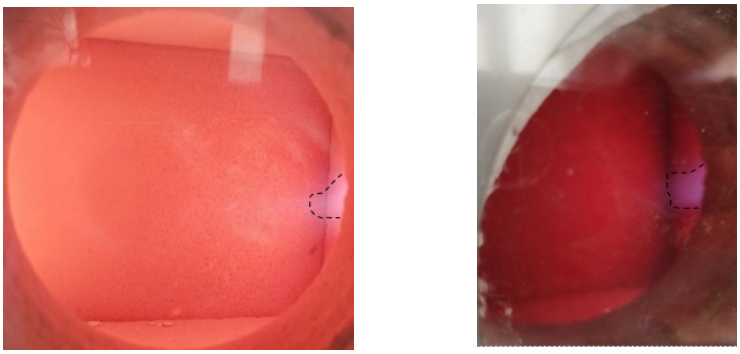

(d) γ = 0.5. **(e)** γ = 0.59.

Figure 9. Flame photographs taken through sidewall observation windows in a series of tests at α = 1.

An exception regarding the reduction of underburning with an increase in γ is a series of tests at α = 1, for which, with a small increase in γ (up to 0.25), the flame becomes brighter and turns yellow. This indicates a significant increase in underburning, which was not observed in the test series at α = 1.45–1.75 and needs an explanation. On the one hand, CO_2 has an inhibitory physical effect (high heat capacity), which decreases burning intensity and, consequently, decreases the length of the flame. On the other hand, CO_2-dilution reduces the flame temperature, which, as shown in the article by Glarborg and Bentzen [30], reduces the formation of CO through the reaction CO_2 (+M) = CO + O (+M) (R1). This is the likely reason for the reduction of underburning, since third-body reactions with CO_2 participation can have both a catalytic and an inhibitory effect on combustion [31, 32], while the most important reaction with the direct CO_2 participation CO + OH = CO_2 + H [31, 33–35], slows down significantly due to a decrease in the concentrations of OH and H radicals with an increase in the concentration of CO_2 [32]. Kinetic studies in the field of CO_2-diluted combustion are mainly focused on the laminar burning velocity and ignition delay time, while the formation of CO has not been sufficiently studied yet. At the same time, some studies show that as the concentration of CO_2 in the mixture increases, CO formation decreases [11, 28, 29]. In any case, the effect of CO_2 concentration on CO formation needs separate kinetic studies. At the same time, our study shows that the effect of CO_2 on the combustion process is dual: underburning decreases with increasing CO_2 concentration, but at a certain value, the flame extinguishes. In that case, with the addition of a small amount of CO_2 to the mixture at α = 1, underburning

increases dramatically due to the sudden appearance of an inhibitory effect. With a further increase in the CO_2 supply, the catalytic effect of CO_2 increases faster than the inhibitory one, which leads to a decrease in underburning. In the tests at $\alpha = 1.45$ and 1.75, an increase in underburning was not observed, since the inhibitory effect of CO_2 was compensated by the catalytic effect of additional oxygen.

According to the results of the experiment, the flame extinction limits were determined by the values of α and γ. It was found that the flame extinguishes at $\gamma > 0.7$ under $\alpha = 1$, and at $\gamma > 0.6$ under $\alpha = 1.45$–1.75. For the test series No. 1 at $\alpha = 1$, the results obtained are in good agreement with the article by Saanum and Ditaranto [11], which found that the flame extinction boundary during CO_2-diluted oxy-fuel combustion and atmospheric pressure at $\alpha = 1$ is 78% by the volume of CO_2 in the oxidizer, which corresponds to 70% by mass or $\gamma = 0.7$. It is also noteworthy that under model conditions, the extinction limit is much lower than under full-scale supercritical conditions. According to the article by Iwai et al. [7, 8], at a pressure of 30 MPa and an outlet temperature of 1,400 °C, oxy-fuel combustion is possible with a CO_2 content in the oxidizer of up to 80% by mass (that is, at $\gamma = 0.8$). However, it has not been established whether this value is the limit.

The change in extinction limits with respect to CO_2 content with increasing oxygen excess or pressure needs to be explained. The effect of oxygen and CO_2 on the combustion process in relation to pressure can be divided into a physical and a chemical effect. With increasing oxygen excess, the oxidizer flow rate increases and, accordingly, its velocity also increases, which leads to flame separation. With increasing pressures, the density of the oxidizer strongly increases and, accordingly, its velocity decreases, which allows one to achieve stable combustion at a higher proportion of CO_2 in the mixture. This is the physical effect of oxygen on the limits of flame extinction based on the CO_2 content in the mixture.

The chemical effect of excess oxygen, CO_2, and high pressures on the flame extinction limits based on CO_2 concentration requires more careful consideration. As a number of studies show [32, 33, 36], the most important reactions for methane combustion are $H + O_2 = H + OH$ (R1) and $H + O_2 (+M) = HO_2 (+M)$ (R2). These two reactions are responsible for the formation of most of the H, OH, and HO_2 radicals that actively participate in the oxidation process, while reactions R1 and R2 compete with each other. R2, unlike R1, is very sensitive to both pressures and CO_2 concentrations, which leads to the displacement of H· and OH· reactions by HO_2· reactions at high pressures and CO_2 dilutions. Another feature of R2 is that it can have both a catalytic and an inhibitory effect on combustion, depending on the oxygen excess [32]. In oxygen-rich mixtures, the concentration of CH_3 radicals is greatly reduced, which slows down one of the most important catalytic reactions: $CH_3 + HO_2 = OH + CH_3O$ (R3). For this reason, a higher proportion of HO_2 is converted into low-active H_2O_2 according to reaction $2\ HO_2 = H_2O_2 + O_2$ (R4), which slows combustion down. In this case, the production of additional HO_2 according to reaction R2 only slows oxidation down, which makes reaction R2 inhibitory at $\alpha > 1$. This causes a narrowing of the flame extinction limits based on γ with increasing α: to enhance the inhibitory reaction R2 to the level of flame extinction, a lower concentration of CO_2 is required.

As for the effect of high pressures, it also lies in the field of HO_2-chemistry: with increasing pressure, the R2 reaction sharply intensifies, which, accordingly, leads to an increase in the concentration of HO_2 radicals and a decrease in the concentration of H and OH radicals. Thus, at 500 atm, HO_2 radicals are formed at a rate 10 times faster than H or OH radicals [36]. An increase in the concentration of CO_2 further enhances the R2 reaction and leads to the formation of greater quantities of HO_2, intensifying all the corresponding HO_2 reactions. Due to the abundance of HO_2 radicals, at ultra-high pressures, it becomes possible to maintain stable combustion at higher CO_2 concentrations than at atmospheric pressure. However, the formation of active HO_2 radicals has a limit, after which, with a further increase in CO_2, the flame extinguishes due to CO_2's physical effects. Thus, the change in the limits of flame extinction by the concentration of CO_2 in the oxidizer with a change in pressure and excess oxygen is due to both the physical and chemical effects of CO_2, O_2, and high pressures. Flame extinguishing due to the low temperature of carbon dioxide is excluded, since it was heated before mixing with oxygen, and the temperature of the resulting oxidizing mixture was controlled by thermocouples and did not fall below 32 °C (see **Table 2**). The discovered influence of the oxidizer supply rate on the boundaries of stable combustion must be taken into account when designing burner devices for oxygen-fuel combustion chambers.

In addition to visual observations of the flame, the temperature profile in the combustion chamber was also obtained during the tests. The layout of the measuring thermocouples is shown in **Figure 3**, and the measurement results are shown in **Figure 10**.

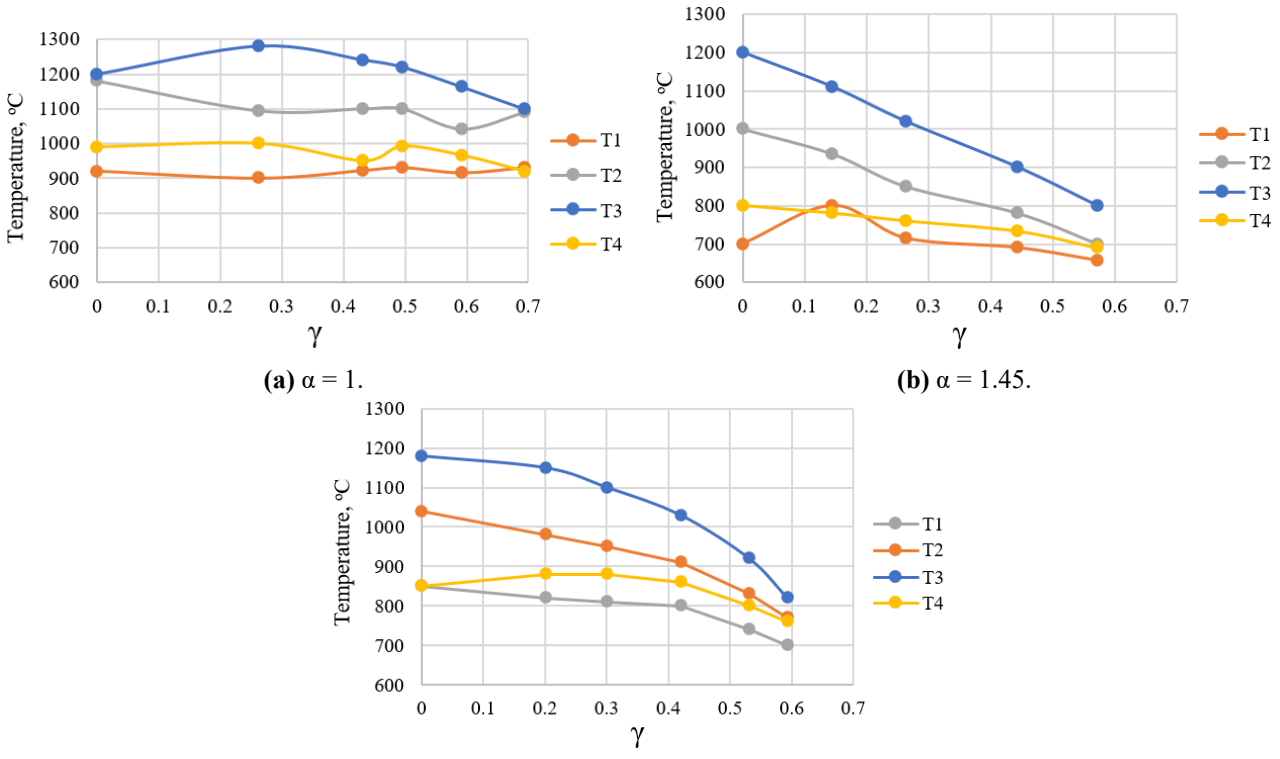

(a) α = 1. **(b)** α = 1.45.

(c) α = 1.75.

Figure 10. Experimental temperature profiles obtained.

As can be seen from **Figure 10**, with an increase in the content of both CO_2 (γ) and O_2 (α) in the mixture, all measured temperatures decrease, which is due to the dilution of the mixture with nonflammable components and is expected. The faster decrease in temperatures at α = 1.45 (**Figure 10b**) compared to other tests is due to a slightly lower preheating of the combustor (see **Table 2**), which intensified heat loss to the environment. We do not see any other explanation for the observed phenomenon, since fuel flow rate practically did not change during the tests, while the flow rates of oxidizer and diluent varied in accordance with α and γ. The observed phenomenon of temperature fluctuations at γ > 0.4 in the test series at α = 1 (**Figure 10a**), which is not observed at α = 1.45–1.75 (**Figure 10b,c**), is also of interest. It is likely that at α = 1 and γ = 0.4 the temperatures reached constant values, while the jumps in temperatures T2 and T3 are due to measurement errors. In the case of test series at α = 1.45–1.75 (**Figure 10b,c**), the flame temperature decreases steadily with increasing γ. This is likely due to the fact that in oxygen-rich mixtures, the inhibitory effect of CO_2 is more significant, since at α > 1, one of the most important reactions involving CO_2, R2, becomes inhibitory (see above), which contributes to the decrease in temperature. In any case, this phenomenon needs its own investigation.

Calculated maximum flame temperatures based on the experimental results are shown in **Figure 11**. These temperature data were used to calculate the criteria of similarity based on the experimental results.

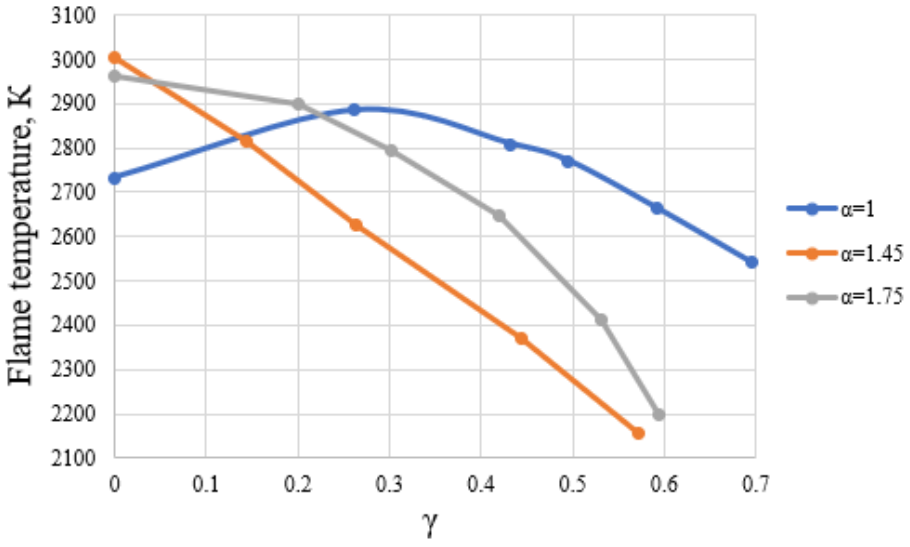

Figure 11. Maximum flame temperatures estimated based on experimental results.

4. Comparison of similarity criteria in model and full-scale conditions

4.1. Methodology for calculating similarity criteria

Based on the experiment, the similarity criteria were evaluated in full-scale conditions and in experimental model conditions. The calculation task was to determine the dependence of the similarity criteria between the model and full-scale operating conditions, depending on the content of O_2 (α) and CO_2 (γ) in the model mixture.

The similarity criteria for the study were selected in accordance with the paper by

Osipov et al. [15]. The analysis of the equations of conservation of mass, momentum, thermal energy, and transport of impurities has shown that the following similarity criteria are most important for the combustion process: Re, Eu, Fr, Pe, Bo, Da_1, Sh, and Da_3. The Froude number is the ratio of gravity to inertia forces and can be omitted because during combustion, gravity is weak compared to inertia. Also, Pe and Sh can be replaced by Pr and Sc, respectively, since Pe = Pr · Re and Sh = f(Re, Sc). Thus, the following similarity criteria were considered: Re, Eu, Pr, Sc, Bo, Da_1, and Da_3. Re and Eu are responsible for hydrodynamic similarity, Pr and Sc for similarity of thermophysical properties, and Bo, Da_1, and Da_3 for similarity of heat exchange and chemical properties. A brief description of all the similarity criteria under consideration is presented in **Table 3**.

Table 3. Similarity criteria important for combustion.

Criteria	Formula	Physical meaning
	Hydrodynamics	
Reynolds number	$\mathrm{Re} = \frac{v \cdot d}{\nu}$, where ν is kinematic viscosity, $\frac{\mathrm{m}^2}{\mathrm{s}}$; v is velocity, $\frac{\mathrm{m}}{\mathrm{s}}$; d is hydraulic diameter, m.	Ratio of viscous forces to inertia forces
Euler number	$\mathrm{Eu} = \frac{\Delta p}{\rho \cdot v^2}$, where Δp is pressure drop, Pa; ρ is density, $\frac{\mathrm{kg}}{\mathrm{m}^3}$.	Ratio of pressure forces to inertia forces
	Thermophysical properties	
Prandtl number	$\mathrm{Pr} = \frac{\mu \cdot c_p}{k}$, where μ is dynamic viscosity, Pa · s, c_p is specific heat capacity, $\frac{\mathrm{J}}{\mathrm{kg} \cdot \mathrm{K}}$, k is thermoconductivity, $\frac{\mathrm{W}}{\mathrm{m} \cdot \mathrm{K}}$.	Similarity of temperature and velocity fields
Schmidt number	$\mathrm{Sc} = \frac{\nu}{D}$, where D is diffusion coefficient, $\frac{\mathrm{m}^2}{\mathrm{s}}$	Ratio of the molecular transfer of the amount of motion to the diffusion transfer of the mass of impurities
	Thermal and chemical effects	
Boltzmann number	$\mathrm{Bo} = \frac{\mu \cdot c_p}{\sigma \cdot T^3}$, where T is temperature, K; $\sigma = 5,67 \cdot 10^{-8} \frac{BT}{M^2 \cdot K^4}$ is Stefan-Boltzmann constant.	Ratio of the flow enthalpy to the intensity of heat exchange by radiation
First Damköhler number	$\mathrm{Da}_1 = \frac{d \cdot W}{v \cdot \rho \cdot Y}$, where$W$is reaction rate, $\frac{\mathrm{kg}}{\mathrm{m}^2 \cdot \mathrm{s}}$; Y is concentration of the reactant.	Ratio of the reaction rate to the rate of convective mass transfer
Third Damköhler number	$\mathrm{Da}_3 = \frac{Y \cdot d \cdot \Delta H \cdot k}{T \cdot v \cdot \rho \cdot c_p}$, where ΔH is thermal effect of chemical reaction, k is equilibrium constant.	Ratio of the thermal effect of the reaction to convective energy transfer

For full-scale conditions, the same burner tested in this paper, but operating under full-scale conditions of the Allam cycle (30 MPa, 895 K) at γ = 0.804 and α = 1.05, was used. γ = 0.804 was chosen because this value roughly corresponds to the operating conditions of a full-scale Allam cycle combustion chamber in steady state from the article by Iwai et al. [7]. From experimental tests of full-scale combustion chambers [6–9], it is difficult to determine the experimentally used value of α; α = 1.05 was adopted, since it is necessary to ensure complete combustion of the fuel with the minimum possible excess oxygen. The pressure drop in the burner to calculate Eu was estimated by the magnitude of pressure losses due to local resistance (sudden expansion), while the reaction rate for the calculation of Da_1 was estimated by the

Arrhenius equation. A comparison of full-scale and model conditions is presented in **Table 4**.

Table 4. Comparison of full-scale and model conditions.

Parameter	Full-scale conditions	Model conditions
Hydraulic diameter, m	0.13	0.13
Methane lower calorific value, $\frac{\text{MJ}}{\text{m}^3}$	37.5	37.5
Thermal power, W	15,000	Measured by gas flow rate
Pressure, MPa	30	0.1
Outlet temperature, K	895	Measured (about 300 K)

The physical properties of the substances involved in the reaction were calculated based on temperature and pressure using the CoolProp database. For the experiment, the maximum flame temperature calculated from the experimental data (see **Figure 9**) was used as the estimation temperature, taking into account the underburning of the fuel during the experiment. For full-scale conditions, the estimation temperature was the adiabatic flame temperature; that is, the completeness of combustion was assumed to be 100%. According to the article by Suzuki et al. [9], in the full-scale conditions of the Allam cycle, the completeness of combustion tends to 100%; therefore, underburning of fuel can be ignored when estimating the maximum flame temperature in full-scale conditions. The adiabatic flame temperature of the mixture under full-scale conditions was estimated iteratively using the standard formula (2), which assumes that there is no underburning (that is, the combustion products are only CO_2 and H_2O in the case of methane combustion) and all the heat of combustion goes for heating combustion products. The numerator corresponds to the sum of the fuel calorific value and the enthalpy of the initial reagents, while the denominator corresponds to the enthalpy of flue gases under adiabatic flame temperature:

$$T_{ad} = \frac{G_{CH_4} \cdot \left(Q_{CH_4} + T_{CH_4} \cdot c_{p_{CH_4}}\right) + G_{O_2}^{init} \cdot T_{O_2}^{init} \cdot c_{p_{O_2}}^{init} + G_{CO_2}^{init} \cdot T_{CO_2}^{init} \cdot c_{pCO_2}^{init}}{G_{O_2}^{prod} \cdot c_{p_{O_2}}^{prod} + G_{CO_2}^{prod} \cdot c_{pCO_2}^{prod} + G_{H_2O}^{prod} \cdot c_{pH_2O}^{prod}}, \quad (2)$$

where G_{CH_4}, $G_{O_2}^{init}$, $G_{CO_2}^{init}$ are flow rates of CH_4, O_2 and CO_2 in the initial mixture;

Q_{CH_4} is the lower calorific value of CH_4, given in **Table 4**;

T_{CH_4}, $T_{O_2}^{init}$, $T_{CO_2}^{init}$ are initial temperatures of CH_4, O_2 and CO_2;

$c_{p_{CH_4}}$, $c_{p_{O_2}}^{init}$, $c_{pCO_2}^{init}$ are isobaric heat capacities of CH_4, O_2 and CO_2 under initial temperature;

$G_{O_2}^{prod}$, $G_{CO_2}^{prod}$, $G_{H_2O}^{prod}$ are flow rates of O_2, CO_2 and H_2O in flue gases;

$c_{p_{O_2}}^{prod}$, $c_{pCO_2}^{prod}$, $c_{pH_2O}^{prod}$ are isobaric heat capacities of O_2, CO_2 and H_2O under adiabatic flame temperatures (estimated iteratively).

The assessment of the adiabatic flame temperature and physical properties of components under full-scale conditions is given in **Table 5**.

Table 5. Physical properties of components under full-scale conditions.

Parameter	CH_4	O_2	CO_2	H_2O	Mixture
Inlet mass fraction	0.045	0.187	0.768	-	1
Initial temperature, K	655.6	387.7	939.1	-	895.4
Outlet mass fraction	0	0.01	0.89	0.1	1
Adiabatic flame temperature, K	1,987.34				
Density ρ, $\frac{kg}{m^3}$	27.34	55.4	75.28	32.32	70.8
Dynamic viscosity μ, Pa·s	$4.6 \cdot 10^{-5}$	$7.83 \cdot 10^{-5}$	$6.55 \cdot 10^{-5}$	$7.21 \cdot 10^{-5}$	$6.62 \cdot 10^{-5}$
Diffusion coefficient *D*, $\frac{m^2}{s}$	0.0253	0.0253	0.0253	0.0253	0.0253
Thermoconductivity λ, $\frac{W}{m \cdot K}$	0.39	0.12	0.33	0.27	0.33
Isobaric heat capacity, $\frac{J}{kg \cdot K}$	6,137.4	1,184.2	1,381	2,883.2	1,529.8

4.2. Results of the similarity criteria calculation

Figures 12 and **13** show graphs of the hydrodynamic similarity criteria (Re and Eu), depending on the test, in comparison with full-scale conditions. As can be seen in **Figure 12**, the Reynolds number in full-scale conditions is much higher than in model conditions. This is due to the high density and, consequently, low kinematic viscosity of flue gases at ultra-high pressures. Under model conditions, an increase in α and γ increases Re, which is associated with an increase in velocity of the mixture due to an increase in oxidizer flow rate and a decrease in kinematic viscosity (the viscosity of CO_2 is lower than that of O_2 or H_2O). Therefore, the closest match in the Reynolds number is observed at the highest components consumption, that is, at α = 1.75 and γ = 0.69, where the discrepancy is only 12.3%. The experimental α and γ, however, are quite far from the full-scale ones (α = 1.05, γ = 0.804). An increase in γ improves convergence in Re, while a decrease in α decreases convergence. Thus, if it is possible to ensure oxy-fuel combustion under model conditions at γ more than 0.7, then it will be possible to ensure similarity at lower α, that is, closer to full-scale conditions.

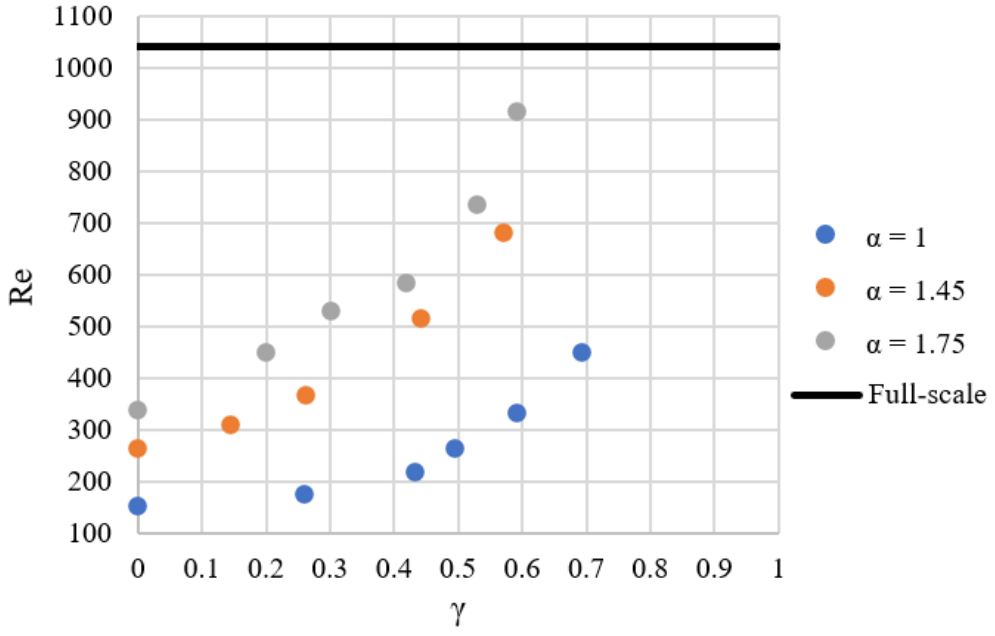

Figure 12. Dependence of the Reynolds number in experimental conditions on α and γ.

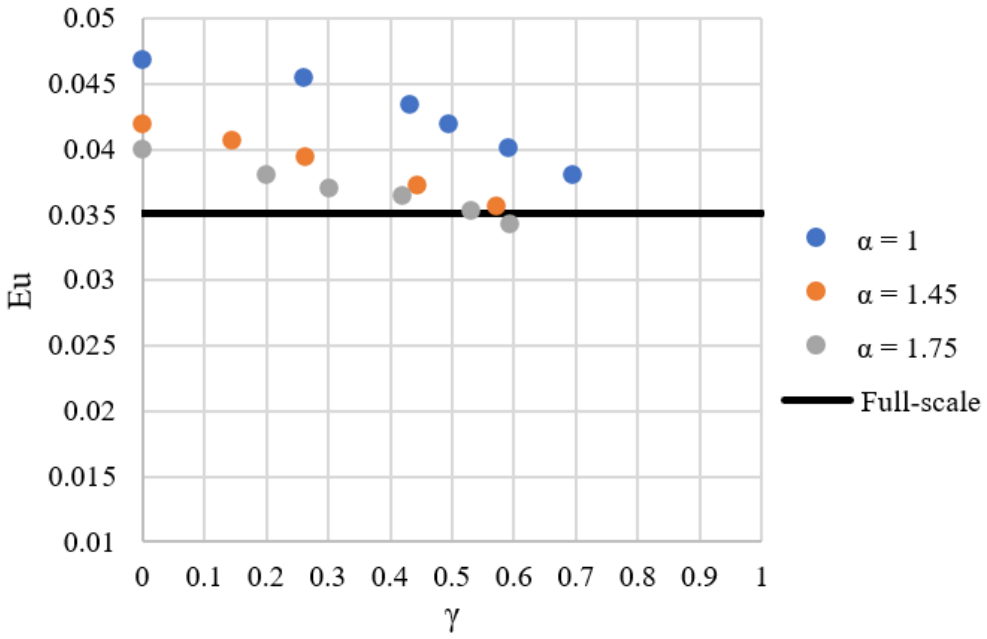

Figure 13. Dependence of the Euler number in experimental conditions on α and γ.

As for the Euler number, as can be seen from **Figure 13**, the model Euler number is quite higher than the full-scale one. This is due to higher velocity in model conditions caused by relatively low density. With an increase in γ and α, the model Eu decreases, converging with the full-scale value, which is caused by an increase in density (CO_2 has a higher density than O_2 and H_2O) and velocity due to higher γ and oxidizer flow rates. Consequently, the minimum deviation from full-scale conditions (no more than 10%) for the Euler number is also observed at maximum component flow rates, that is, at γ = 0.5–0.6 for α = 1.45–1.75, and also at γ = 0.7 for α = 1. The effect of α and γ on the convergence between model and full-scale conditions is similar to Re. As in the case of Re, if it is possible to achieve stable combustion at γ > 0.7 in model conditions, then the similarity by Euler number may be achieved at model α and γ close to full-scale ones (α = 1.05, γ = 0.804). In general, it can be concluded that for now, the best hydrodynamic similarity of the experiment with full-scale conditions is provided by the regime at α = 1.75 and γ = 0.69, with the potential to achieve similarity at α = 1.05 and γ = 0.804 after the burner modification.

Figures 14 and **15** show graphs of the similarity criteria characterizing the thermophysical properties of substances—Sc and Pr. The Schmidt number is essentially a ratio of kinematic viscosity to thermal diffusivity, both parameters changing similarly with temperature and pressure. For that reason, model and full-scale Schmidt numbers are close. An increase in α almost does not influence Sc, since excess oxygen concentration in flue gases is relatively low in all cases. At the same time, an increase in γ significantly decreases Sc, since $\frac{v}{D}$ ratio for CO_2 is lower than that of O_2 and H_2O, and CO_2 concentration strongly increases with increasing γ. As can be seen from **Figure 14**, good convergence in the Schmidt number (a discrepancy of no more than 20%) is achieved in all experimental modes, the closest match being at γ = 0.5. Interpolating to full-scale γ (0.804), it can be concluded that similarity by Sc will remain within 20% discrepancy. Therefore, if we are able to achieve stable combustion

at $\gamma > 0.7$ under model conditions, we will also be able to remain close to full-scale α and γ.

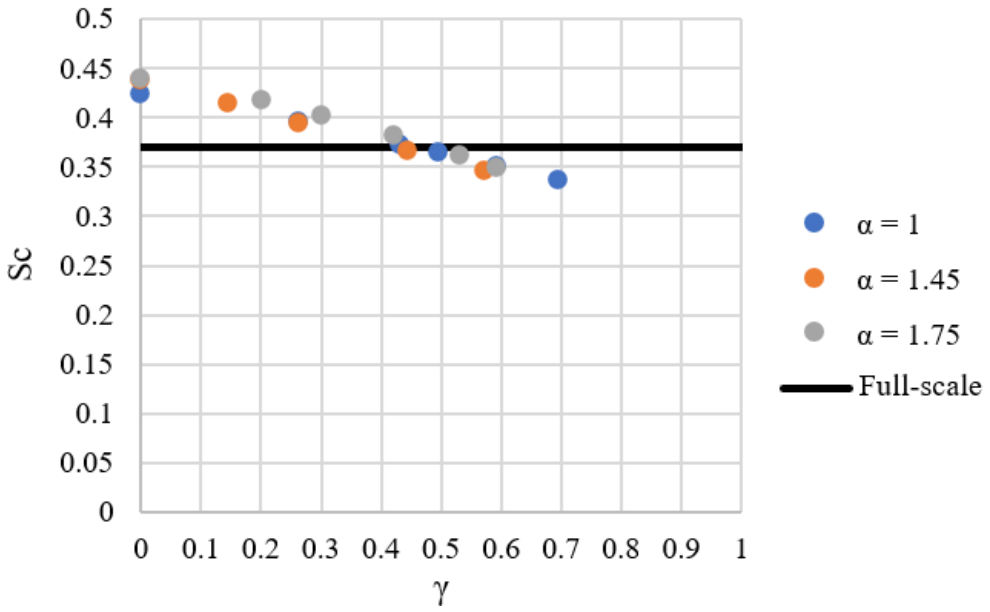

Figure 14. Dependence of the Schmidt number in experimental conditions on α and γ.

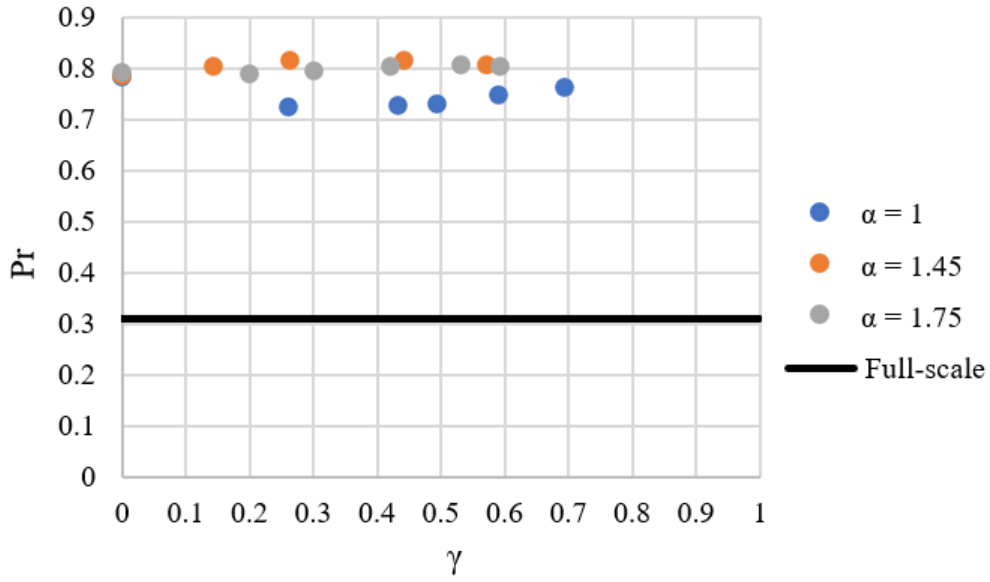

Figure 15. Dependence of the Prandtl number in experimental conditions on α and γ.

As for the Prandtl number, as can be seen from **Figure 15**, the experimental agreement with the full-scale conditions is much worse, as the experimental points are about 2.5 times higher than the full-scale values. At the same time, α and γ almost do not influence Pr, since Pr strongly depends on the phase of substance (supercritical fluid vs normal gas), that is, on temperature and pressure. However, it should be noted that qualitative similarity remains in both model and full-scale conditions: $Pr < 1$, which indicates the dominance of thermal diffusion over viscous forces. Thus, it can be concluded that an acceptable convergence of experimental results with full-scale thermophysical properties is observed in all experimental modes.

Figures 16–18 show the graphs of the similarity criteria characterizing the thermal

and chemical effects: Bo, Da_1, and Da_3. The Boltzmann number depends on dynamic viscosity, temperature, and heat capacity. In both model and full-scale conditions, heat capacities are close, while μ almost does not depend on pressure, and full-scale temperature is lower than the model one due to higher γ. That's the reason why, as can be seen in **Figure 16**, full-scale Bo is much higher than the model one. An increase in γ and α lowers the temperature, thus converging the model burner to a full-scale one. As can be seen from **Figure 16**, according to the Boltzmann number, a good convergence (discrepancy no more than 20%) is observed at γ and α, which are as close as possible to the full-scale regime (α = 1.05, γ = 0.804), that is, at γ = 0.69 and α = 1, as well as at γ = 0.2–0.3 at α = 1.45–1.75. Interpolating γ to 0.804 at α = 1, we can conclude that in this case, the model and full-scale Boltzmann numbers would be almost identical.

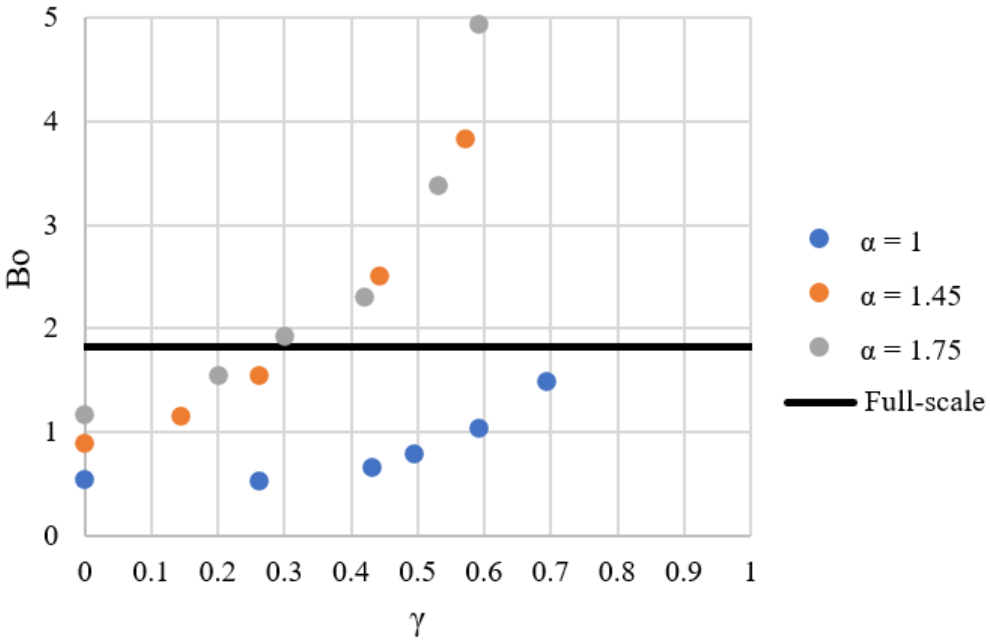

Figure 16. Dependence of the Boltzmann number in experimental conditions on α and γ.

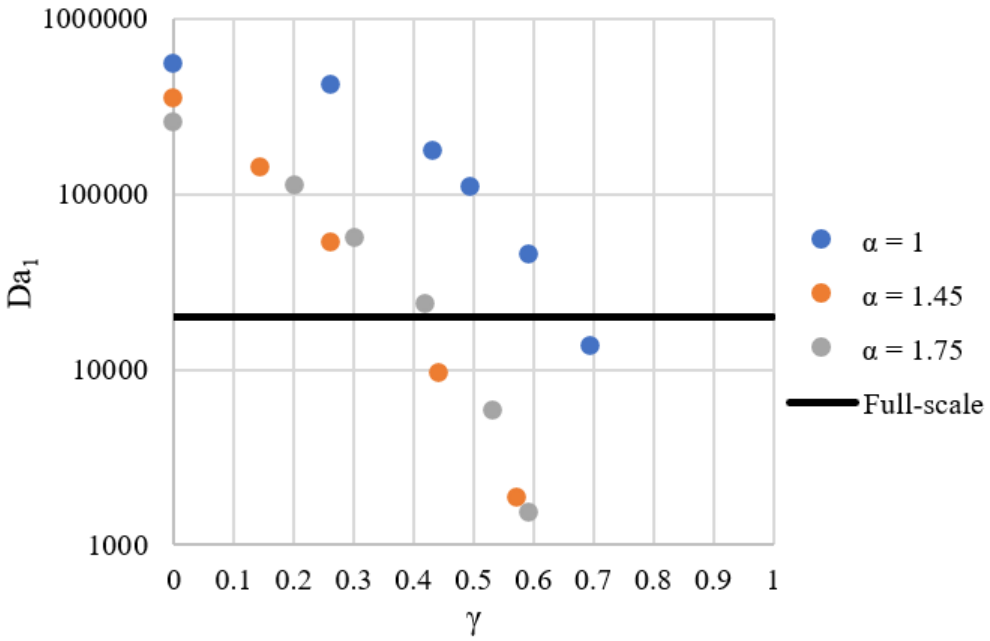

Figure 17. Dependence of the first Damköhler number in experimental conditions on α and γ.

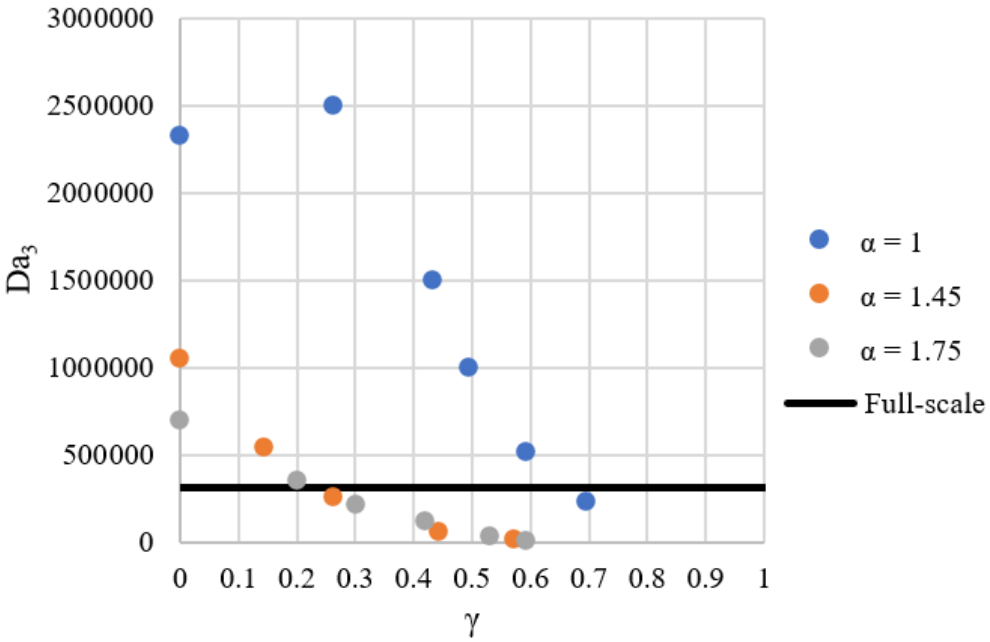

Figure 18. Dependence of the third Damköhler number under experimental conditions on α and γ.

As for the first Damköhler number, as can be seen from **Figure 17**, Da_1 decreases with increasing α and γ, which is due to both a decrease in the reaction rate due to the addition of excess oxygen and ballast CO_2 to the mixture, and an increase in convective mass transfer due to an increase in oxidizer flow rate. As can be seen from **Figure 17**, a good agreement with the full-scale conditions (discrepancy no more than 20%) is also observed for γ = 0.2–0.3 under α = 1.45–1.75. However, under γ = 0.69 and α = 1, the discrepancy reaches 50%. But it should be noted that the qualitative similarity of the processes is preserved, since preserved is the order of magnitude (10,000–20,000): in both full-scale and model conditions, the reaction rate is much higher than the mass transfer rate.

For the third Damköhler number (**Figure 18**), it decreases with an increase in α and γ, since the thermal effect of reaction is consistent, while the energy transfer rate increases with an increase in the oxidizer flow rate. For the model Da_3, the level of agreement with the full-scale conditions is similar: discrepancy no more than 20% at γ = 0.2–0.3 for α = 1.45–1.75 and a qualitative convergence at γ = 0.69 and α = 1 (for Da_3, the discrepancy reaches 30%). Thus, it can be concluded that an acceptable convergence of experimental tests with full-scale conditions by thermal and chemical effects is observed at γ = 0.69 for α = 1 and at γ = 0.2–0.3 for α = 1.45–1.75. But interpolation of experimental results to full-scale α and γ (1.05 and 0.804) shows that in that case, similarity by thermal and chemical effects can't be achieved.

Thus, based on the results of calculating the similarity criteria in full-scale (30 MPa, 895 K at inlet) and model experimental conditions (0.1 MPa, about 300 K at inlet), it was found that agreement on hydrodynamics (Re, Eu) is observed in the mode γ = 0.6 at α = 1.75, agreement of thermophysical properties is observed in all experimental modes, and agreement of thermal and chemical effects is observed at γ = 0.2–0.3 for α = 1.45–1.75 and at γ = 0.69 for α = 1. At γ = 0.6 and α = 1.75, for which similarity with full-scale conditions in hydrodynamics is achieved,

similarity in heat exchange processes is not observed: Bo (4.9 vs. 1.8), Da_1 (1,526 vs. 19,941), and Da_3 (12,420 vs. 313,043) differ by an order of magnitude. At the same time, in the regimes at γ = 0.2–0.3 for α = 1.45–1.75 and at γ = 0.69 for α = 1, which are characterized by agreement on thermal and chemical effects, there is agreement on the number of Eu (the discrepancy does not exceed 20%) and qualitative agreement on the number of Re (stable laminar regime), which allows to conclude about hydrodynamic similarity. Thus, it has been experimentally established that varying the values of α and γ in the mixture under model normal conditions makes it possible to reduce the discrepancy between all significant similarity criteria compared with full-scale supercritical conditions. This confirms the possibility of using the results of model studies to verify mathematical models made for designing full-scale oxy-fuel combustion chambers of direct-fired supercritical CO_2 cycles.

5. Conclusion

According to the results of experimental tests of the 15 kW model oxy-fuel burner in a tunnel furnace at atmospheric pressure, it was established:

1) At atmospheric pressure, the limit of the mass fraction of CO_2 in the oxidizer γ, at which combustion of the oxy-fuel mixture is possible, is 0.7 at α = 1 and 0.6 at α = 1.45–1.75. The limit γ for higher α is lower due to an increase in the rate of oxidizer velocity, which leads to flame separation. The flame extinction limit obtained during these tests is much lower than for full-scale supercritical combustion chambers (at least 0.8 according to the article by Nomoto et al. [6]);
2) The dual effect of CO_2-dilution has been experimentally confirmed. On the one hand, the addition of CO_2 reduces the intensity of combustion, resulting in a lower length of the flame. On the other hand, the addition of CO_2 greatly reduces underburning, which results in a decrease in flame brightness and a change of its color from white to blue. Thus, the inhibitory effect of CO_2 affects the combustion process as a whole, and the catalytic effect affects afterburning;
3) At α = 1, an exception to this rule was found: with a small increase of γ to 0.25, the underburning increased, and a bright yellow flame formed. However, with the further growth of γ, the underburning decreased, and the color of the flame changed to blue. At α = 1.45–1.75, no such phenomenon was observed, since the inhibitory effect of CO_2 was interrupted by the catalytic effect of additional O_2;
4) It is established that at atmospheric pressure and α = 1 at γ > 0.4, an unstable combustion regime is observed, which is reflected in chaotic temperature changes. With an increase in α, the unstable mode disappears – the flame extinction occurs from the stable mode;
5) The main similarity criteria of combustion (Re, Eu, Pr, Sc, Bo, Da_1, Da_3) for full-scale supercritical and model experimental conditions are calculated. It was found that changing α and γ for the model mixture relative to the full-scale mixture makes it possible to reduce the discrepancy between the similarity criteria. It was found that the experimental combustion mode at α = 1 and γ = 0.69 under model conditions (0.1 MPa, about 300 K at the inlet) is similar to the full-scale conditions (30 MPa, 895 K, α = 1.05, γ = 0.804). This proves the possibility of experimentally

investigating full-scale oxy-fuel combustion under model conditions.

In the future, it is planned to use the results obtained for the verification of numerical simulation techniques for oxy-fuel combustion.

Author contributions: Conceptualization, SO and PB; methodology, SO and PB; software, PB; validation, PB and VY; formal analysis, PB and VY; investigation, PB; resources, SO and NR; data curation, SO and PB; writing—original draft preparation, PB, VY and IF; writing—review and editing, SO and VY; visualization, VY and IF; supervision, SO and PB; project administration, SO and NR; funding acquisition, SO and NR. All authors have read and agreed to the published version of the manuscript.

Funding: This study was supported by the Russian Science Foundation under Agreement No. 23-79-10291, https://rscf.ru/project/23-79-10291/.

Institutional review board statement: Not applicable.

Informed consent statement: Not applicable.

Data availability statement: The data will be made available on request.

Conflict of interest: The authors declare no conflict of interest.

AI use statement: The authors declare that no artificial intelligence (AI) tools were used in the preparation of this manuscript.

References

1. Emissions. Available online: https://www.statista.com/markets/408/topic/949/emissions/ (accessed on 21 February 2026).
2. Allam R, Martin S, Forrest B, et al. Demonstration of the Allam Cycle: An Update on the Development Status of a High Efficiency Supercritical Carbon Dioxide Power Process Employing Full Carbon Capture. Energy Procedia. 2017; 114: 5948–5966. doi: 10.1016/j.egypro.2017.03.1731
3. What's new in GRI-Mech 3.0. Available online: http://combustion.berkeley.edu/gri-mech/version30/text30.html (accessed on 21 February 2026).
4. Komarov I, Kharlamova D, Makhmutov B, et al. Natural Gas-Oxygen Combustion in a Super-Critical Carbon Dioxide Gas Turbine Combustor. E3S Web of Conferences. 2020; 178: 01027. doi: 10.1051/e3sconf/202017801027
5. Hu X, Yu Q, Liu J, et al. Investigation of laminar flame speeds of $CH4/O_2/CO_2$ mixtures at ordinary pressure and kinetic simulation. Energy. 2014; 70: 626–634. doi: 10.1016/j.energy.2014.04.029
6. Nomoto H, Itoh M, Brown W, et al. ICOPE-15-1176 Cycle and Turbine Development for the Supercritical Carbon Dioxide Allam Cycle. In: Proceedings of the International Conference on Power Engineering (ICOPE); 30 November–4 December 2015; Yokohama, Japan. doi: 10.1299/jsmeicope.2015.12._ICOPE-15-_112
7. Iwai Y, Itoh M, Morisawa Y, et al. Development Approach to the Combustor of Gas Turbine for Oxy-Fuel, Supercritical CO_2 Cycle. In: Proceedings of the ASME Turbo Expo 2015: Turbine Technical Conference and Exposition; 15 June 2015; Montreal, QC, Canada. doi: 10.1115/GT2015-43160
8. Iwai Y, Itoh M. Gas turbine combustor for supercritical carbon dioxide cycle. Toshiba Reviews. 2015; 70: 16–19. (in Japanese)
9. Suzuki S, Iwai Y, Itoh M, et al. High pressure combustion test of gas turbine combustor for 50MWth supercritical CO_2 demonstration power plant on Allam cycle. In: Proceedings of the International Gas Turbine Congress; 17–22 November 2019; Tokyo, Japan.
10. Anderson R, Hustad C, Skutley P, et al. Oxy-fuel Turbo Machinery Development for Energy Intensive Industrial Applications. Energy Procedia. 2014; 63: 511–523. doi: 10.1016/j.egypro.2014.11.056
11. Saanum I, Ditaranto M. Experimental Study of Oxy-fuel Combustion under Gas Turbine Conditions. Energy & Fuels.

2017; 31(4): 4445–4451. doi: 10.1021/acs.energyfuels.6b03114
12. Weber R, Mancini M. On scaling and mathematical modelling of large scale industrial flames. Journal of the Energy Institute. 2020; 93(1): 43–51. doi: 10.1016/j.joei.2019.04.010
13. Prieler R, Mayr B, Demuth M, et al. Application of the steady flamelet model on a lab-scale and an industrial furnace for different oxygen concentrations. Energy. 2015; 91: 451–464. doi: 10.1016/j.energy.2015.08.070
14. Osipov S, Komarov I, Zlyvko O, et al. Investigation of the parameters influence of the oxy-fuel burner and the test bench parameters on the deviation of the model similarity criterions from the full-scale values. Applied Chemical Engineering. 2024; 7(1). doi: 10.24294/ace.v7i1.2802
15. Osipov SK, Bryzgunov PA, Shaikh MM, et al. Influence of the experimental setup parameters on the deviation of the similarity criteria in the experimental study of the model boundary conditions from the similarity criteria of the full-scale combustion chamber. Applied Chemical Engineering. 2025; 8(1). doi: 10.59429/ace.v8i1.5645
16. Skubic L, Gyergyek S, Huš M, et al. A review of multiscale modelling approaches for understanding catalytic ammonia synthesis and decomposition. Journal of Catalysis. 2024; 429: 115217. doi: 10.1016/j.jcat.2023.115217
17. Lotrič A, Sekavčnik M, Pohar A, et al. Conceptual design of an integrated thermally self-sustained methanol steam reformer —High-temperature PEM fuel cell stack manportable power generator. International Journal of Hydrogen Energy. 2017; 42(26): 16700–16713. doi: 10.1016/j.ijhydene.2017.05.057
18. Lašič Jurković D, Liu JL, Pohar A, et al. Methane Dry Reforming over Ni/Al_2O_3 Catalyst in Spark Plasma Reactor: Linking Computational Fluid Dynamics (CFD) with Reaction Kinetic Modelling. Catalysis Today. 2021; 362: 11–21. doi: 10.1016/j.cattod.2020.05.028
19. Harkou E, Adamou P, Al-Salem SM, et al. Computational fluid dynamics (CFD) modelling as a power multiplier tool for the design improvement of gaseous and liquid fuels: current status, challenges and perspectives. Fuel. 2026; 404: 136401. doi: 10.1016/j.fuel.2025.136401
20. Nesterov PM, Osipov SK, Komarov II, et al. Vortex Burner Device. RU 231576 U1, 31 January 2025.
21. PD100I-DA2.5-111-0.25 Model 1x1 High-Reliability Pressure Sensor for Primary Production. Available online: https://owen-kapo.ru//products/pd100i-da25-111-025 (accessed on 21 February 2026). (in Russian)
22. DTPK254-17.80/200/0.5K.1 TCMS (Thermocouple Cable with Mineral Insulation in a Steel Sheath)-Based Thermocouples with Cable Output. Available online: https://owen-kapo.ru//products/dtpk254-178020005k1 (accessed on 21 February 2026). (in Russian)
23. EE741—Technical description for the flow meter EE 741 for compressed air and gases. Available online: https://epluse.nt-rt.ru/images/manuals/EE741.pdf (accessed on 21 February 2026). (in Russian)
24. Thermoscope 300. Available online: https://www.rospribor.com/files/698/195e21d202/tehnicheskie-harakteristiki-pirometra-termoskop-300-2c.pdf (accessed on 21 February 2026). (in Russian)
25. DTPS thermocouples “platinorhodium-platinum”, modification DTPS021.1E-0.5/0.21. Available online: https://owen-prom.ru/products/dtps-termopary-iz-blagorodnykh-metallov/?mod=684275 (accessed on 21 February 2026). (in Russian)
26. VA 520—Insertion flow meter. Available online: https://air.by/upload/iblock/9a1/v3x126o3u9pi2den3ndn151f1qzxohbg.pdf?ysclid=mmxjojxsz2967028737 (accessed on 21 February 2026). (in Russian)
27. Kutateladze SS, Borishansky VM. Heat Transfer Handbook. Gosenergoizdat; 1958. Available online: https://djvu.online/file/JcS7cS5GCUXkN?ysclid=mnyi0fl0y0178912821 (accessed on 21 February 2026). (in Russian)
28. Amato A, Hudak R, Noble DR, et al. Methane Oxy-Combustion for Low CO_2 Cycles: Measurements and Modeling of CO and O_2 Emissions. In: Proceedings of the ASME Turbo Expo 2010: Power for Land, Sea, and Air; 10 October 2010; Glasgow, UK. pp. 213–222. doi: 10.1115/GT2010-22300
29. Li B, Shi B, Chu Q, et al. Characteristics of stoichiometric $CH_4/O_2/CO_2$ flame up to the pure oxygen condition. Energy. 2019; 168: 151–159. doi: 10.1016/j.energy.2018.11.039
30. Glarborg P, Bentzen LLB. Chemical Effects of a High CO_2 Concentration in Oxy-Fuel Combustion of Methane. Energy & Fuels. 2008; 22(1): 291–296. doi: 10.1021/ef7005854
31. Hu X, Yu Q, Liu J. Chemical effect of CO_2 on the laminar flame speeds of oxy-methane mixtures in the condition of various equivalence ratios and oxygen concentrations. International Journal of Hydrogen Energy. 2016; 41(33): 15068–15077. doi: 10.1016/j.ijhydene.2016.05.276
32. Xia W, Huang C, Yang J, et al. Experimental and modeling study of ignition delay times of natural gas with CO_2 dilution. Fuel. 2024; 358: 130148. doi: 10.1016/j.fuel.2023.130148
33. Liu Y, Zou C, Cheng J, et al. Experimental and Numerical Study of the Effect of CO_2 on the Ignition Delay Times of Methane under Different Pressures and Temperatures. Energy & Fuels. 2018; 32(10): 10999–11009. doi:

10.1021/acs.energyfuels.8b02443

34. Zhong F, Li Q, Ding X, et al. Experimental and chemical kinetics analysis on the combustion behaviors and flame instabilities of diluted methane/air mixtures. International Journal of Heat and Mass Transfer. 2024; 232: 125957. doi: 10.1016/j.ijheatmasstransfer.2024.125957
35. Shang R, Zhuang Z, Yang Y, et al. Laminar flame speed of H_2/CH_4/air mixtures with CO_2 and N_2 dilution. International Journal of Hydrogen Energy. 2022; 47(75): 32315–32329. doi: 10.1016/j.ijhydene.2022.07.099
36. Zhukov VP, Sechenov VA, Starikovskii AYu. Spontaneous Ignition of Methane–Air Mixtures in a Wide Range of Pressures. Combustion, Explosion and Shock Waves. 2003; 39(5): 487–495. doi: 10.1023/A:1026186231905